Journal of Solid State Chemistry **167,** 446–452 (2002)
doi:10.1006/jssc.2002.9653

Pressure and Temperature Dependence of the Ferroelectric–Paraelectric Phase Transition in $PbTiO_3$

A. Sani and M. Hanfland

European Synchrotron Radiation Facility, BP 220, F-38043 Grenoble, France
E-mail:sani@esrf.fr

and

D. Levy

Dipartimento di Scienze Mineralogiche e Petrografiche, Università di Torino, via Valperga Caluso 25, I-10125 Torino, Italy
E-mail:levy@dsmp.unito.it

Received January 23, 2002; in revised form April 11, 2002; accepted May 10, 2002

Synchrotron X-ray powder diffraction patterns were collected at the European Synchrotron Radiation Facility (ESRF, Grenoble, France) on powder samples of $PbTiO_3$ (tetragonal, $Z = 1$ *P4mm* $a = 3.9036(1)$ Å and $c = 4.1440(2)$ Å at room conditions) applying external pressure using a diamond anvil cell. Data were collected at four different temperatures (room temperature, 462, 538 and 623 K) up to the phase transition to the cubic phase ($Z = 1$, *Pm3m* $a = 3.8647(4)$ Å at RT and 11.6 GPa). Analyzing the behavior of the cell parameters obtained by the Rietveld refinement, we were able to extract the dependence of the critical temperature on external pressure. The bulk moduli of the lead titanate were calculated for the first time. The progressive decrease of the distortion of the Pb and Ti coordination polyhedra with pressure allows to propose a structural explanation of the first-/second-order cross-over in the ferroelectric–paralectric phase transition on applying pressure.

Key Words: **high pressure; phase transition; ferroelectric; perovskite.**

1. INTRODUCTION

$PbTiO_3$ is one of the more interesting and more studied perovskites possessing a ferroelectric phase under ambient conditions. The strong interest in this compound is caused by its high spontaneous polarization and the wide temperature stability of the ferroelectric phase: the ferroelectric-paraelectric phase transition temperature (763 K) (1) is the highest in the family of ferroelectric perovskites.

Above 763 K $PbTiO_3$ is cubic (1), while at room conditions it shows a tetragonal phase with a c/a ratio of 1.063 (2), (Fig. 1). The enhancement of the ferroelectric properties and of the deviation from the cubic structure in $PbTiO_3$ with respect to the very similar $BaTiO_3$ and $SrTiO_3$ is probably to be found in the presence of lead. Pb is not an alkaline earth metal and it is more deformable and polarizable than Ba and Sr. Moreover, as emphasized by Megaw (3) the directional character of the Pb–O bond, possessing a covalent component, could be also responsible for the large axial ratio and the high Curie point.

The ferroelectric–paraelectric phase transition was extensively studied in the last decades by several different experimental techniques and computational methods and it has been considered as a purely displacive ferroelectric phase transition (4) for a long time. Recently, Sicron *et al.* (5) observed the presence of local distortions above T_C revealing nonnegligible order–disorder character of the phase transition, confirming the results obtained by means of Raman spectroscopy (6) and neutron scattering (7).

Under pressure the transition temperature of ferroelectric perovskites decreases (8). In the specific case of $PbTiO_3$ the phase transition loses its first-order character and gradually becomes a second-order phase transition. This has been proved experimentally by Raman scattering (9) which allowed to observe a second-order ferroelectric-paraelectric phase transition at 12.1 GPa at room temperature. The cross-over between the two different phase transition types was attributed to the proximity of the tricritical point to ambient conditions in $PbTiO_3$ (10).

We have undertaken an X-ray diffraction study at different temperatures to obtain direct structural

0022-4596/02 $35.00

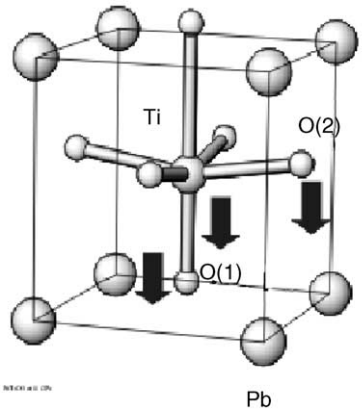

FIG. 1. Tetragonal structure of $PbTiO_3$. The arrows refer to the direction of the displacement of the atoms in approaching the phase transition.

information about the pressure-induced transition, in order to find a structural explanation for the crossover in the order of the phase transition.

2. EXPERIMENTAL

The compression of the sample was performed in a membrane-type diamond anvil cell. The diameter of the diamond culet was of 300 μm for the experiments at room temperature and of 600 μm for the isotherms collected at 462, 538 and 623 K. A stainless-steel gasket with a 125 μm hole diameter was used for the experiment at room temperature (RT), while for the high-temperature (HT) runs inconel gaskets with 250 μm diameter holes were employed. $PbTiO_3$ sample was synthesized by sol–gel route, described in detail elsewhere (11, 12). The finely grown powder was placed in the gasket hole with nitrogen (RT) and silicon oil (HT) as pressure transmitting media. Angular dispersive X-ray diffraction experiments were performed at ID9 of the ESRF (Grenoble, France) at a fixed wavelength of 0.41436 Å. The beam was focussed to $30 \times 30\ \mu m^2$, using a Pt-coated Si-mirror for the vertical focussing and an asymmetrically cut bent Si(111) Laue monochromator for the horizontal one (13). The diamonds, mounted with a thrust axis parallel to the incident beam, allowed to collect a diffraction cone of about 25° in 2θ. The pressure on the sample was determined before and after each imaging, by monitoring the fluorescence line shift of a small ruby pellet enclosed in the DAC with the sample (14). Due to the high dependence of the ruby fluorescence line width on temperature, the $^7D_0$–$^5F_0$ fluorescence line of the SrB_4O_7:Sm^{2+} (15) was used as pressure gauge during data collection at high temperatures. XRD patterns were collected at room temperature in the pressure range 0–37 GPa with steps of about 1 GPa and up to the tetragonal-cubic phase transition at 462, 538 and 623 K. 2D-XRD patterns were collected on a MAR345 image plate with a pixel dimension of $100 \times 100\ \mu m^2$. With this setup the angular resolution calibrated on Si-NBS, was of 0.04°. The images were treated and integrated using the software FIT2D (16) and the structural refinement of integrated patterns was achieved through the Rietveld method as implemented in the GSAS software package (17) (Fig. 2). The origin of the tetragonal phase was chosen at the Pb site and the refinements were performed starting from the coordinates reported in Ref. (18), that is Pb at (0,0,0), Ti at ($\frac{1}{2}$, $\frac{1}{2}$, $\frac{1}{2}$+ z(Ti)), O(1) at ($\frac{1}{2}$, $\frac{1}{2}$, z(O(1))) and O(2) ($\frac{1}{2}$, 0, $\frac{1}{2}$+ z(O(2))). In the cubic phase, the Ti atom is at the center of the cell, while the oxygen atoms center the cubic face. Correction for anomalous dispersion of Pb atoms was applied, using the values of −1.407 and 4.007 for f' and f'', respectively (obtained from tabulated data). Pseudo-Voigt profile function proved to be appropriate to fit the experimental pattern and no asymmetry correction was applied. The background was modelled using a 12-term expansion of the Chebychev polynomial function. Table 1 sets out the results of the Rietveld refinements for selected values of pressure and temperature.

3. RESULTS AND DISCUSSION

Figure 3 shows the dependence of the unit-cell parameters with the applied pressure at room temperature. Lead titanate results to be more compressible along the c-axis, with respect to a. The observed a values have been fitted by a second-order polynomial in p (i.e., $\sum_{j=0}^{3} c_j p^j$) whose coefficients result, $c_0 = 3.9059(5)$ Å, $c_1 = -0.0016(3)$ Å GPa^{-1} and $c_2 = -0.0002(1)$ Å GPa^{-2}. On the contrary, c is properly fitted by the third-order polynomial in p whose coefficients are $c_0 = 4.133(2)$ Å, $c_1 = -0.053(2)$ Å GPa^{-1}, $c_2 = 0.0049(5)$ Å GPa^{-2} and $c_3 = -0.0002(0)$ Å GPa^{-3}. Our results up to 6.35 GPa are in quite good agreement with the previously reported low-pressure values (19).

The tetragonal–cubic phase transition takes place at 11.2 GPa. The difference with the value of 12.1 GPa reported by Raman spectroscopy studies (9) could be due to the different pressure medium used. No post-cubic phase transition, as recently observed in $KNbO_3$ (20), was detected up to 37 GPa. It is interesting to observe that the width of the doublets remains constant with pressure, so the overlapping originates from a progressive coalescence of close peaks and not from peak broadening, like in the case of $KNbO_3$ (21). This, among with the absence of any hysteresis effect, confirms that the pressure-induced ferroelectric–paraelectric phase transition at room temperature has a second-order character.

From the p–V data obtained it is possible to extract the elastic parameters of $PbTiO_3$. The bulk moduli of both

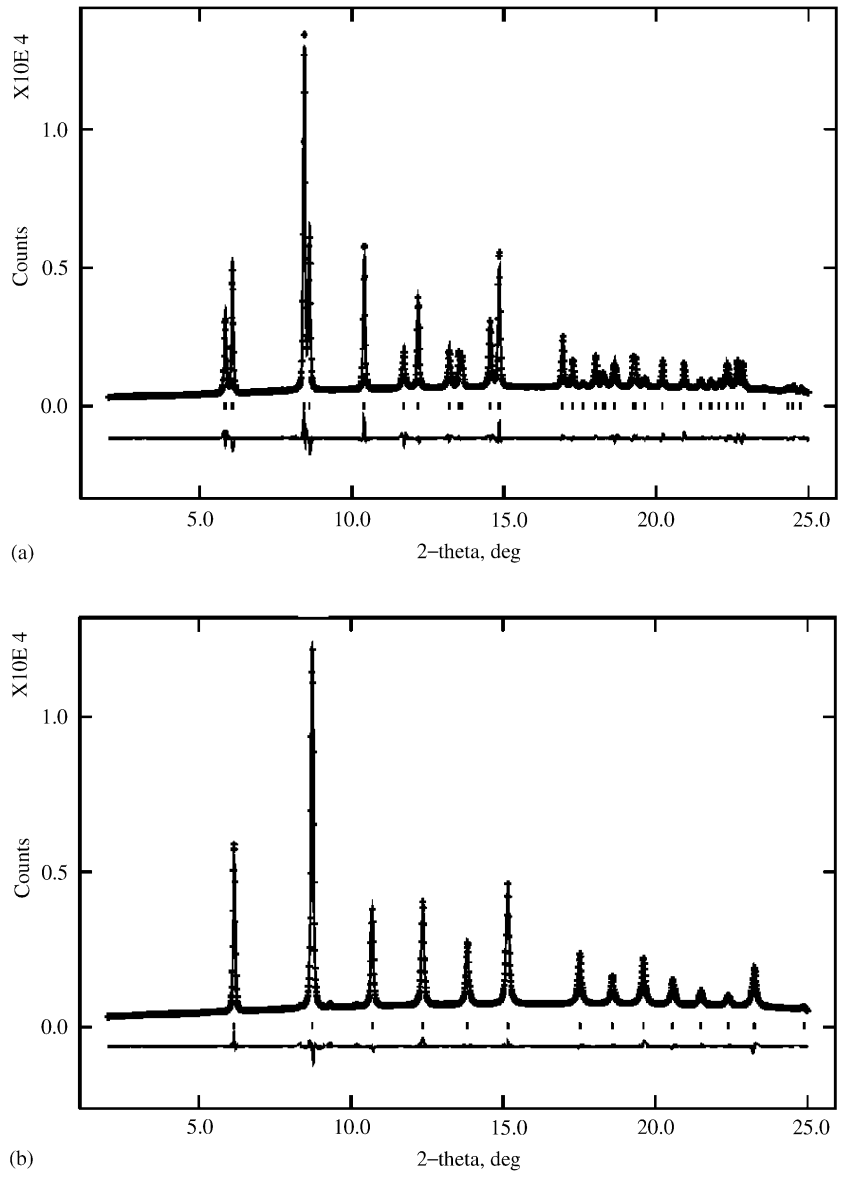

FIG. 2. Experimental (crosses), calculated and difference profiles of the pattern of the tetragonal phase at 3.32 GPa (above) and of the cubic phase at 14 GPa (below). Both diffractograms were collected at room temperature.

the tetragonal and the cubic phases were obtained using a third-order Birch–Murnaghan equation of state (22), using the program EOSFIT (23). The values fitted for the tetragonal phase are $K_0 = 107(3)$ GPa and $K' = 5.0(1)$ with $K'' = -0.05\,\mathrm{GPa}^{-1}$ implied value, while for the cubic phase we obtained $K_0 = 237(4)$ GPa and $K' = 4.5(1)$ with

TABLE 1
Summary of the Rietveld Refinement Parameters at Selected Pressures and Temperatures

T (K)	p (GPa)	a (Å)	c (Å)	z(Ti)	z(O(1))	z(O(2))	R_P(%)	wR_P(%)	R_{obs}(%)
RT	2.17	3.9023(1)	4.0329(1)	0.022(2)	0.084(4)	0.090(3)	3.05	4.43	5.02
462	3.10	3.9123(1)	3.9901(1)	0.040(2)	0.066(3)	0.059(2)	1.66	2.76	5.35
538	2.85	3.9155(2)	4.0034(3)	0.026(4)	0.098(6)	0.066(6)	6.18	8.63	6.83
623	2.00	3.9304(1)	3.9600(1)	0.050(1)	0.065(5)	0.058(4)	2.46	1.44	8.80

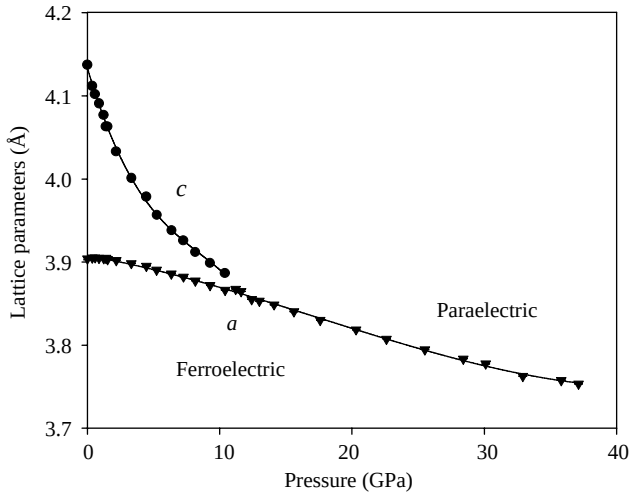

FIG. 3. Pressure dependence of the the cell parameters of $PbTiO_3$ at room temperature. The error bars are omitted since smaller than the symbol size.

$K'' = -0.05\,\mathrm{GPa}^{-1}$ implied value. The tetragonal phase of $PbTiO_3$ results to be more compressible with respect to $BaTiO_3$ and of $KNbO_3$, which show a bulk modulus of 150 and 170 GPa, respectively (21). On progressively applying temperature, some changes in the behavior of the system with pressure are detectable.

Figure 4 shows the dependence of the unit-cell parameters upon applied pressure at 462, 538 and 623 K, where it is evident that temperature influences the behavior of $PbTiO_3$ under pressure. The most striking effect is the lowering of the critical pressure on raising temperature. This behavior was already predicted by Samara (8), but, in contrast with the results reported in the reference cited, we see a linear dependence of T_C on p. Indeed, the value of dT_C/dp of $-40(2)\,\mathrm{K\,GPa}^{-1}$ obtained from our data is quite different from the value of $-84\,\mathrm{K\,GPa}^{-1}$ reported in (8). These discrepancies, however, could be justified by the difference in the experimental conditions; the result reported in Ref. (8) was obtained by dielectric loss

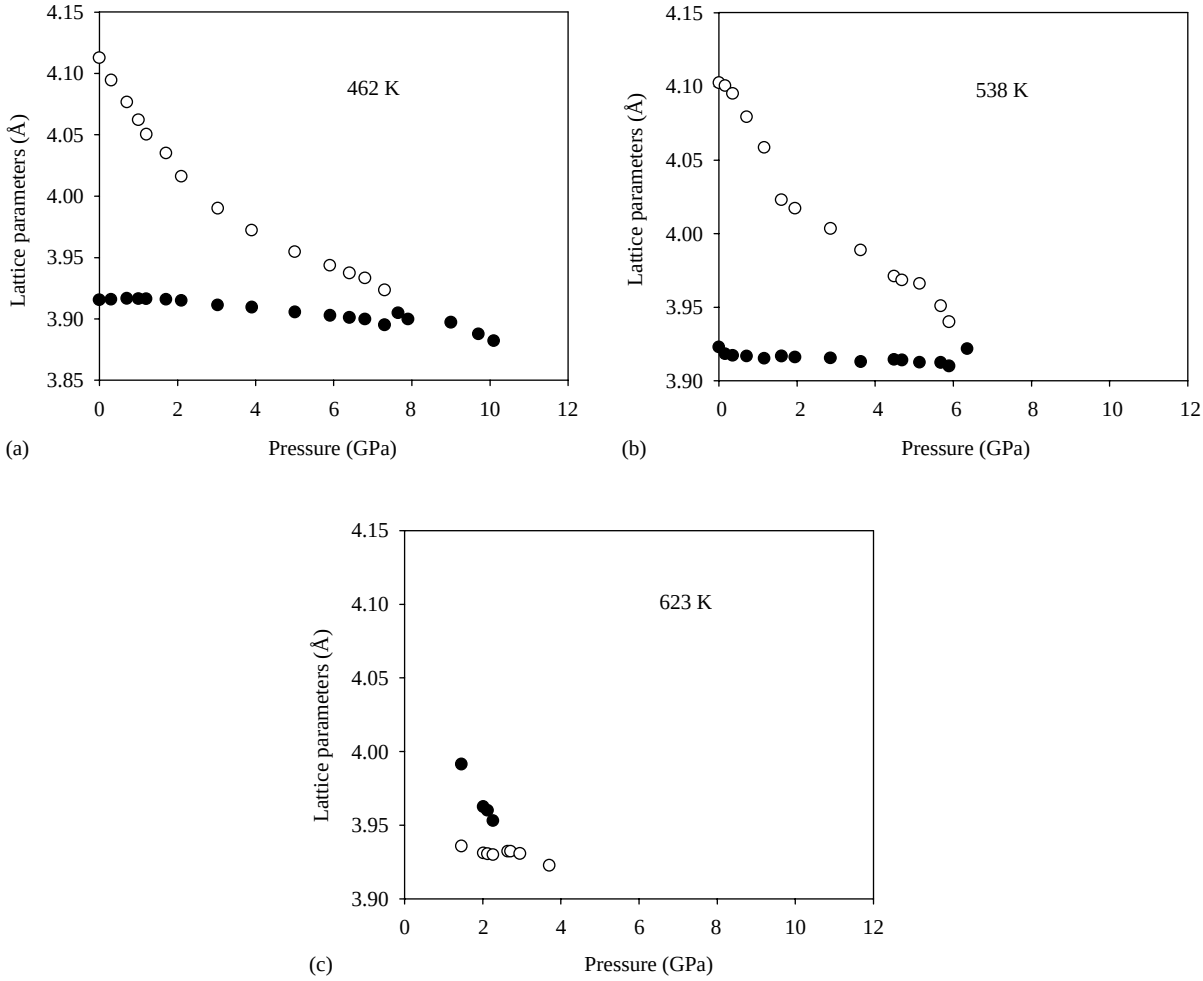

FIG. 4. Evolution of the cell parameters under applied pressure at different temperatures: (a) 462 K, (b) 538 K, (c) 623 K. The p-axis length scale was kept equal for all the plots to highlight the lowering of the critical pressure. The error bars are omitted since smaller than the symbol size.

measurements at very low pressure (not exceeding 2.4 GPa). For all the temperatures considered, the *c*-axis results to be more compressible than the *a*-axis. Besides that, the dependence of the *c*-axis on pressure seems to undergo major changes on raising temperature. We do not remark differences in the evolution of the *c*-axis with pressure at 462 K: the *p–c* curve can be easily fitted by a third-order polynomial whose coefficients are quite similar to that obtained for the same curve at room temperature ($c_0 = 4.111(2)$ Å, $c_1 = -0.059(2)$ Å GPa^{-1}, $c_2 = 0.0077(6)$ Å GPa^{-2} and $c_3 = -0.0004(1)$ Å GPa^{-3}). Figure 4(b), reporting the evolution of the cell parameters at 538 K, shows a clear change of slope at about 1.5 GPa in the evolution of the *c*-axis with pressure. It seems that under 1.5 GPa the behavior of the *c*-axis with pressure has no link with the trend of the *c*-axis at lower temperatures, while above 1.5 GPa we can recognize the third polynomial trend. At 623 K, the range of stability of the tetragonal phase is very small, preventing any proper fitting of the lattice parameters as a function of *p*. In the range before the phase transition, the behavior of the *c*-axis at 623 K is very similar to that at 538 K at low pressure. It seems likely that at 538 K a "high-temperature" behavior is present, while above 1.5 GPa *c* shows a "low-temperature" trend.

These changes in the evolution of the cell parameters with pressure at different temperatures can be better highlighted by the calculation of the spontaneous strain defined as $z^{1/2} = (c/a - 1)^{1/2}$. As it is shown in Fig. 5, on increasing temperature, $z^{1/2}$ changes its dependence on pressure. The curve at room temperature shows no change of slope, while the one at 538 K show a change of slope at about 1.5 GPa. Again, at 623 K we do not observe any change of slope. We can also observe that the curve at 538 K shows at low pressure the same behavior of the curve at 623 K, while at higher pressure we find the slope observed at room temperature. Ramirez *et al.* (10) stated the presence of a cross-over between the two types of phase transition (first and second order) and located it at 1.8 GPa at room temperature. The results here reported are in agreement with this statement, since the change of slope of $z^{1/2}$ has often been interpreted as an indication of a change in the order of the phase transition (7).

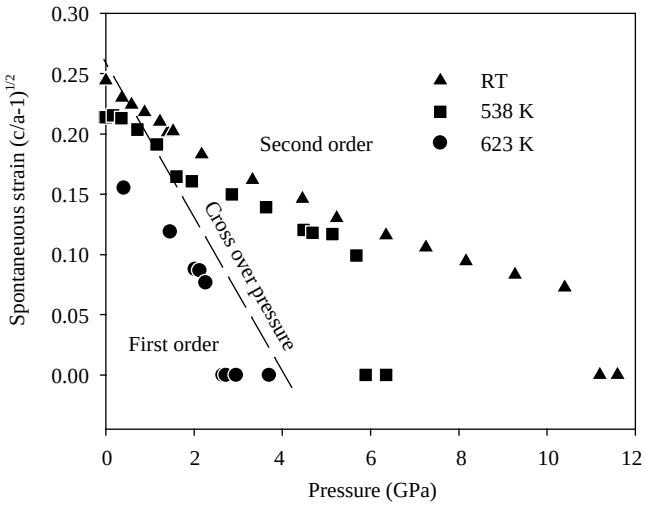

FIG. 5. Spontaneous strain pressure dependence at selected temperatures. The dashed line shows a possible temperature dependence of the cross-over pressure. The error bars are omitted since smaller than the symbol size.

The absence of a change of slope in $z^{1/2}$ at room temperature is not in contrast with Ref. (10): it could be likely that the cross-over point determined theoretically by Ramirez is shifted towards low pressures at room temperature and that the change of slope is undetectable. The curve at 623 K confirms our statement. In fact, this last shows no change of slope, meaning that the cross-over pressure at which the $z^{1/2}$ starts a linear dependence on *p* is located above the phase transition. In this scenario, we can actually suppose a temperature dependence of the cross-over pressure as reported in Fig. 5.

The order parameter of the phase transition is the spontaneous polarization P_S which can be obtained, neglecting the electronic polarization, from $P_S^i(p) = 1/V_0 \times \sum_i \varepsilon_i q_i \delta S_i(p)$, where V_0 is the cell volume, ε_i the fraction of cations of *i*th kind with charge q_i and δz_i the displacement of the *i*th cation from the center of the oxygen environment (24). In this work, the spontaneous polarization was calculated using the cationic displacements obtained by the Rietveld refinement and using the formal cationic charge of the atoms, assuming the crystal to be purely ionic. The value obtained at ambient conditions is about 59 μC cm^{-2}, which is in perfect agreement with the value of 57 μC cm^{-2} obtained by Rameika and Glass (25) by means of pyroelectric measurements. Figure 6 reports also the dependence of the spontaneous polarization with pressure at room temperature and at 623 K. At room temperature P_S shows no jump at the phase transition, evidencing a second-order character. On the contrary at 623 K we observe a typical first-order jump. This result confirms the presence of a cross-over (p, T) point where the phase transition changes from first to second order. If we compare the behavior of the spontaneous polarization with that of the spontaneous strain, we observe the presence of a jump at all temperatures. This is not in contrast with the presence of the cross-over. The spontaneous strain gives a measure of the "tetragonality" of the system and derives directly from the cell parameters values, while the spontaneous polarization is calculated taking into account the position of the atoms besides the cell parameters.

Since the spontaneous polarization is directly linked to the distortion of the Ti and Pb coordination polyhedra we can discuss the *p*, *T* behavior of the spontaneous polarization in terms of the distortion of the polyhedra

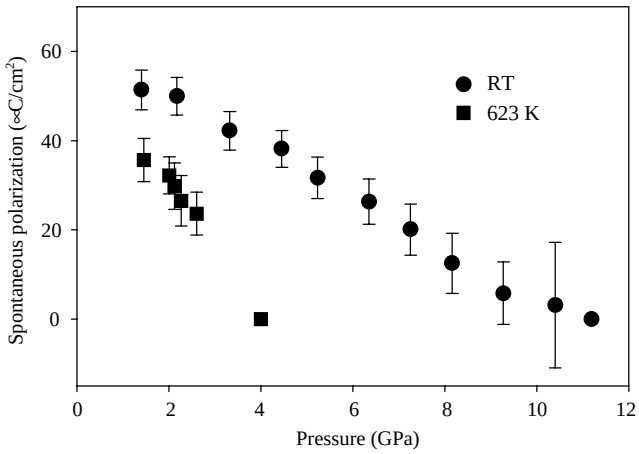

FIG. 6. Pressure dependence of the spontaneous polarization calculated by Rietveld refined parameters at room temperature and 623 K.

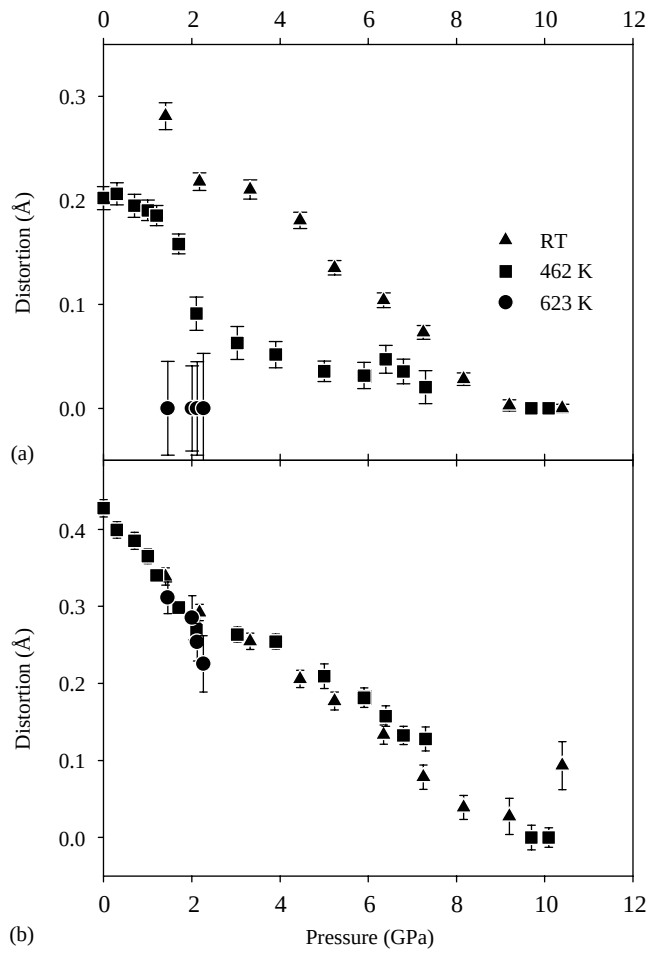

FIG. 7. Distortion of the coordination polyhedra as function of the pressure and of the temperature: (a) Ti octahedron; (b) Pb dodecahedron.

(Table 2). Figure 7(a), shows the pressure dependence of the distortion of Ti octahedron at different temperatures and Fig. 7(b) the distortion of the Pb dodecahedron at the same values of p and T. At room temperature and at 462 K the distortion of the coordination polyhedra goes progressively to zero on applying pressure, in contrast of what was supposed in previous structural refinements where a constant ratio between the cationic shifts was imposed (26). The evolution of the distortion of the coordination polyhedra with pressure shows a remarkable change of slope at about 3 GPa, both for Ti and Pb. This change of slope is linked to the difference in shift of the cations: at low pressure, Ti atoms seem not influenced by the external conditions, on the contrary the distortion of the Pb dodecahedra decreases strongly. Above 3 GPa, there is an inversion of the phenomena, since the distortion of the Ti octahedra starts diminishing strongly and one of the Pb polyhedra shows a less steep evolution towards zero. It could be likely that the Ti atoms response to pressure starts to be significative above 3 GPa, pressure at which the Pb shifts start showing a less remarkable dependence on pressure.

At 623 K the behavior of the distortion changes: the distortion of the Ti octahedron is almost equal to zero at all values of pressure, while the distortion of the Pb polyhedron shows a slight decrease with pressure and a value of 0.23 Å at the phase transition. These results and the absence of any Raman activity in the cubic phase (9) lead to conclude that on applying pressure at room temperature the order–disorder contribution is absent or at least strongly reduced and no tetragonal domains are present in cubic phase. At high temperatures, the distortion of the polyhedra is not such pressure dependent, and the polyhedra start to behave as rigid units, as already

TABLE 2
Bond Distances at Selected Temperatures and Pressures

T (K)	p (GPa)	Ti–O(1) (Å)	Ti–O(1) (Å)	Ti–O(2) (Å)	O(2)–Ti–O(2) (°)	Pb–O(1) (Å)	Pb–O(2) (Å)	Pb–O(2) (Å)	O(2)–Pb–O(2) (°)
RT	2.17	1.76(1)	2.27(1)	1.970(1)	164(1)	2.780(2)	2.56(1)	2.56(1)	99.4(7)
462	3.10	1.89(2)	2.09(2)	1.957(1)	175(1)	2.779(2)	2.63(1)	2.96(1)	96.0(6)
538	2.85	1.71(3)	2.29(1)	1.964(2)	171(1)	2.796(3)	2.62(1)	2.99(2)	96.9(6)
623	2.00	1.92(2)	2.03(2)	1.965(1)	178(2)	2.791(3)	2.63(2)	2.96(2)	96.6(9)

observed in the cubic phase at high temperatures (18). The nonzero distortion at the phase transition was an indication of the presence of tetragonal domains in the cubic phase (5,6) and of a nonnegligible order–disorder character of the phase transition.

The possible model of the behavior of $PbTiO_3$ at high pressures could be found starting by the model proposed by Sicron *et al*. (5) for the phase transition at T_C at room pressure. On increasing temperature the disorder starts to be consistent, especially at Pb site (7) and there is formation of ferroelectric clusters which have a nonzero spontaneous polarization at local scale. The progressive increase of disorder makes the spontaneous polarization of the clusters to be strongly disoriented one to another, so the cubic phase is formed by tetragonal clusters of nonzero polarization at local scale. There is no correlation between the long-range order value and the microscopic value of P_S. High pressure reduces the distortion of the polyhedra and the order/disorder contribution is strongly reduced. There is no formation of tetragonal clusters, or at least their dimensions are so small that the long-range order behavior of the spontaneous polarization reflects the behavior on microscopic scale. As soon as the temperature is increased, the disorder effect starts to be nonnegligible and there is a competitive effect between the reduction of distortion induced by pressure and the increase of disorder induced by temperature.

4. CONCLUSIONS

In this work we reported the structural study of $PbTiO_3$ at high pressure at different temperatures. This study allowed to assess the structural behavior at the phase transition and consequently an explanation of the cross-over between the first- and second-order character of the ferroelectric–paraelectric phase transition. The order parameter of the phase transition P_S has two correlation length scales: the first is related to the dimension of the tetragonal domains, the second is related to the microscopic spontaneous polarization. When no domain is formed, or at least they are very small in dimension, the two correlation length scales coincide and the transition is second order. When the dimension of the tetragonal domains is so big that the average on long-range order of P_S is very different from the value of the spontaneous polarization at microscopic scale, we observe an abrupt drop to zero of the order parameter, so a first-order phase transition. The cross-over takes place when the dimension of the cluster reaches a critical value, which gives rise to a difference in the two correlation length scale values of P_S.

ACKNOWLEDGMENTS

The authors thank M. Catti and T. Le Bihan for the critical reading of the manuscript. D. Bersani is kindly acknowledged for providing the sample. Three anonymous referees, who contributed substantially to the improvement of the manuscript are thanked for their careful and constructive review.

REFERENCES

1. A. M. Glazer and S. A. Mabud, *Acta Crystallogr. B* **34,** 1065–1069 (1978).
2. G. Shirane, R. Pepinsky, and B. C. Frazer, *Acta Crystallogr.* **9,** 131–140 (1956).
3. H. D. Megaw, *Acta Crystallogr.* **7,** 187–194 (1954).
4. G. Burns and B. A. Scott, *Phys. Rev. B* **7,** 3088–3101 (1973)
5. N. Sicron, B. Ravel, Y. Yacoby, E. A. Stern, F. Dogan, and J. J. Rehr, *Phys. Rev. B* **50,** 13 168–13 180 (1994).
6. M. D. Fontana, H. Hidrissi, and K. Wojcik, *Europhys. Lett.* **11,** 419–424 (1990).
7. R. J. Nelmes, R. O. Plitz, W. F. Kuhs, Z. Tun, and R. Restori, *Ferroelectrics* **108,** 165–170 (1990).
8. G. A. Samara, *Ferroelectrics* **2,** 277–289 (1971).
9. J. A. Sajurio, E. López-Cruz, and G. Burns, *Solid State Commun.* **48,** 221–224 (1983).
10. R. Ramirez, M. F. Lapeña, and J. A. Gonzalo, *Phys. Rev. B* **42,** 2604–2606 (1990).
11. D. Bersani, P. P. Lottici, A. Montenero, S. Pigoni, and G. Gnappi, *J. Mater. Sci.* **31,** 3153–3157 (1996).
12. L. Lan, A. Montenero, G. Gnappi, and E. Dradi, *J. Mater. Sci.* **30,** 3137–3141 (1995).
13. C. Shultze, L. Lienert, M. Hanfland, M. Lorentzen, and F. Zontone, *J. Synchrotron Radiat.* **5,** 77–81 (1998).
14. H. K. Mao, J. Xu, and P. M. Bell, *J. Geophys. Res.* **91,** 4673–4676 (1986).
15. F. Datchi, R. LeToullec, and P. Loubeyre, *J. Appl. Phys.* **81,** 3333–3339 (1997).
16. A. P. Hammersley, S. O. Svensson, M. Hanfland, A. N. Fitch, D. Häusermann, *High Pressure Res.* **14,** 235–248 (1996).
17. A. C. Larsson and R. B. von Dreele, Report LAUR 86–748, Los Alamos National Laboratory, Los Alamos, New Mexico, 1999.
18. R. J. Nelmes and W. F. Kuchs, *Solid State Commun.* **54,** 721–723 (1985).
19. R. J. Nelmes and A. Katrusiak, *J. Phys. C* **19,** L725–730 (1986).
20. K. Kobayashi, S. Endo, T. Ashida, L. C. Ming, and T. Kikegawa, *Phys. Rev. B* **61,** 5819–5822 (2000).
21. J. C. Chervin, J. P. Itié, D. Gourdain, and Ph. Pruzan, *Solid State Commun.* **110,** 247–251 (1999).
22. F. Birch, *J. Geophys. Res.* **57,** 227–286 (1952).
23. R. J. Angel, EOSfit manual BGI-Bayreuth, 2000.
24. M. F. Kuprianov, S. M. Zaitsev, E. S. Gagarina, and E. G. Fesenko, *Phase Transitions* **4,** 55–64 (1983).
25. J. P. Rameika and A. M. Glass, *Mater. Res. Bull.* **5,** 37–46 (1970).
26. R. Ramirez, H. Vincent, R. J. Nelmes, A. Katrusiak, *Solid State Commun.* **77,** 927–929 (1991).